DESIGN AND RESEARCH OF VARIABLE FERTILIZATION SYSTEM FOR RICE BASED ON BILINEAR INTERPOLATION

/

基于双线性插值的水稻变量施肥系统设计与研究

Xiaowei DONG[1*)], Ruixiang LI[1)], Ming Wang[1)], Ximu Zhang[1)], Shunji YU[1)], Jinyi XUE[1)]
[1)] College of Engineering, Heilongjiang Bayi Agricultural University, Daqing/P.R.China
Tel: +86-18745952288; E-mail: dxwai@byau.edu.cn
Corresponding author: Xiaowei DONG
DOI: https://doi.org/10.35633/inmateh-77-121

Keywords: *bilinear interpolation, prescription plot; rice, fertilization device, variable fertilization*

ABSTRACT

To improve fertilization accuracy and uniformity in rice production, a variable-rate fertilization device was designed based on field soil sampling data and model optimization. Ming Shui in Heilongjiang Province, China, was selected as the study area, where soil nutrient data were collected to generate fertilization prescription maps. First, bilinear interpolation was applied to densify the sampling data and enhance spatial continuity, and the interpolation accuracy was evaluated using mean absolute error (MAE = 2.61), root mean square error (RMSE = 4.2), and coefficient of determination (R^2 = 0.74), supplemented by t-tests and Q–Q plot analysis. The results indicated that the method achieved satisfactory accuracy. Subsequently, fertilization prescription maps were generated using the Kriging method in ArcGIS. Based on the fertilization rate range derived from the prescription map, a variable-rate fertilization device equipped with a fertilizer impeller and an adjustable baffle was designed. EDEM simulations and bench tests were conducted to analyze the effects of impeller speed, forward speed, and baffle angle on fertilization uniformity and fertilizer breakage rate. Response surface analysis showed that all factors had significant effects. The optimal parameters were an impeller speed of 65.6 rad/min, a forward speed of 0.39 m/s, and a baffle angle of 54°, resulting in a fertilizer distribution deviation of 8.54% and a breakage rate of 9.16%. Compared with conventional fluted-wheel or pneumatic fertilization devices, the proposed device features two independently adjustable fertilization structures, improving system stability and making it suitable for precision fertilization in paddy fields.

摘要

为提高水稻生产中的施肥精度和均匀性，本文基于田间土壤采样数据与数据优化，设计了一种变量施肥装置。以中国黑龙江省明水县土壤养分数据并生成施肥处方图。首先采用双线性插值法增加采样数据点增强空间连续性，并通过 MAE 为 2.61、RMSE 为 4.2 和 R^2为 0.74 评价插值精度，辅以 t 检验 Q-Q 图分析。表明，该方法具有较高精度。随后利用 ArcGIS 中的 Kriging 方法生成施肥处方图。基于该处方图的施肥量范围，设计了一种配备肥料叶轮和可调挡板的变量施肥装置，并结合 EDEM 仿真与台架试验，分析了叶轮转速、前进速度和挡板角度对施肥均匀性和断条率的影响。结果表明，各因素均具有显著影响。最优解为叶轮转速 65.6 rad/min、前进速度 0.39 m/s、挡板角度 54°，此时施肥变异系数为 8.54%，断条率为 9.16%。与传统槽轮式或气动式施肥装置相比，该装置具有两个可以独立调节肥量的结构，提高了施肥系统的稳定性，适用于精准施肥。

INTRODUCTION

Rice is a major staple crop (*Bin et al., 2023*), and its growth depends on proper nutrient supply (*Li et al., 2021*). Soil fertility often cannot meet nutrient needs at different growth stages, so proper fertilization is important for stable and high yields (*Muthayya et al., 2014; Xu et al., 2015; Liang et al., 2016*). Traditional fertilization does not consider differences between fields or spatial changes within a field (*Sohail et al., 2024; Brambilla et al., 2021*), which can lead to fertilizer waste and uneven nutrient supply.

Prescription map-based variable fertilization technology for rice enables on demand fertilization based on the spatial distribution of soil nutrients, significantly improving fertilizer use efficiency and effectively alleviating agricultural non-point source pollution caused by uneven fertilization (*Niu et al., 2021; Zhou et al., 2023*). The accurate construction of prescription maps is a prerequisite for implementing variable fertilization. *Marti et al*. (*2023*) proposed a nitrogen fertilizer optimization algorithm (NFOA) using remote optical sensors and Sentinel-2 imagery to provide precise, data-driven nitrogen recommendations for rice, supporting the

combined use of chemical and organic fertilizers. *Yu et al. (2022)* developed a UAV-based hyperspectral diagnostic window to accurately identify nitrogen requirements and generate fertilization maps. *Shin et al. (2023)* analyzed spatial variability with a spherical variogram, and produced TN and Av. P_2O_5 distribution maps using kriging interpolation. *Yu et al. (2020)* generated prescription maps for topdressing at the tillering stage based on UAV-recognized minimum operation grids, calculating fertilizer amounts for each grid to enable stage-specific precision fertilization. *Maximilian Lösch et al. (2023)* proposed an algorithm that divides farmland into maneuverable units with assigned fertilization control points, enabling preset fertilization targets and fine-scale control. Overall, despite differences in sensor platforms, algorithms, and map generation methods, existing studies consistently show that data-driven approaches underpin variable-rate fertilization technology.

Overall, the technology for generating prescription maps for rice fertilization has made significant progress. Therefore, further research into variable fertilization structures is of great importance for improving the level of intelligence in rice production. *Qi et al. (2016)* designed a pneumatic variable fertilization machine for paddy fields. Simulation optimization improved the small-hole structure of the air distribution box and mixing joints, enhancing airflow uniformity and fertilizer flow efficiency. *Su et al. (2015)* proposed a variable fertilization system with adjustable slot-roller feed lengths. Using a Kuhn seeder capable of simultaneous sowing and fertilizing, they optimized the mechanical structure for variable application. *Silva et al. (2019)* developed an injection fertilization system for nitrogen management, applying fertilizer according to plant demand and positioning points near the root zone. *Lin et al. (2025)* designed an end-flow acceleration device for compound granular fertilizers based on gas-solid two-phase flow theory, dividing airflow and fertilizer and accelerating air through a tapered pipe to the outlet, which increased deposition velocity and prevented clogging.

In practical paddy fields, soil sampling density is often constrained by field conditions and labor costs, which can reduce the spatial continuity and stability of interpolation when Kriging is used alone. Therefore, bilinear interpolation was first applied to densify the sampling data and smooth local spatial variations, improving the reliability of subsequent Kriging-based prescription maps. Despite progress in pneumatic, mechanical, and injection-based variable fertilization devices, effective integration of structural design and intelligent control remains limited. To address this gap, an impeller-based variable fertilization device integrating prescription map data is proposed. The system regulates fertilizer discharge through real-time control of impeller speed and outlet vane position, enabling precise fertilization adapted to field-specific requirements.

MATERIALS AND METHODS

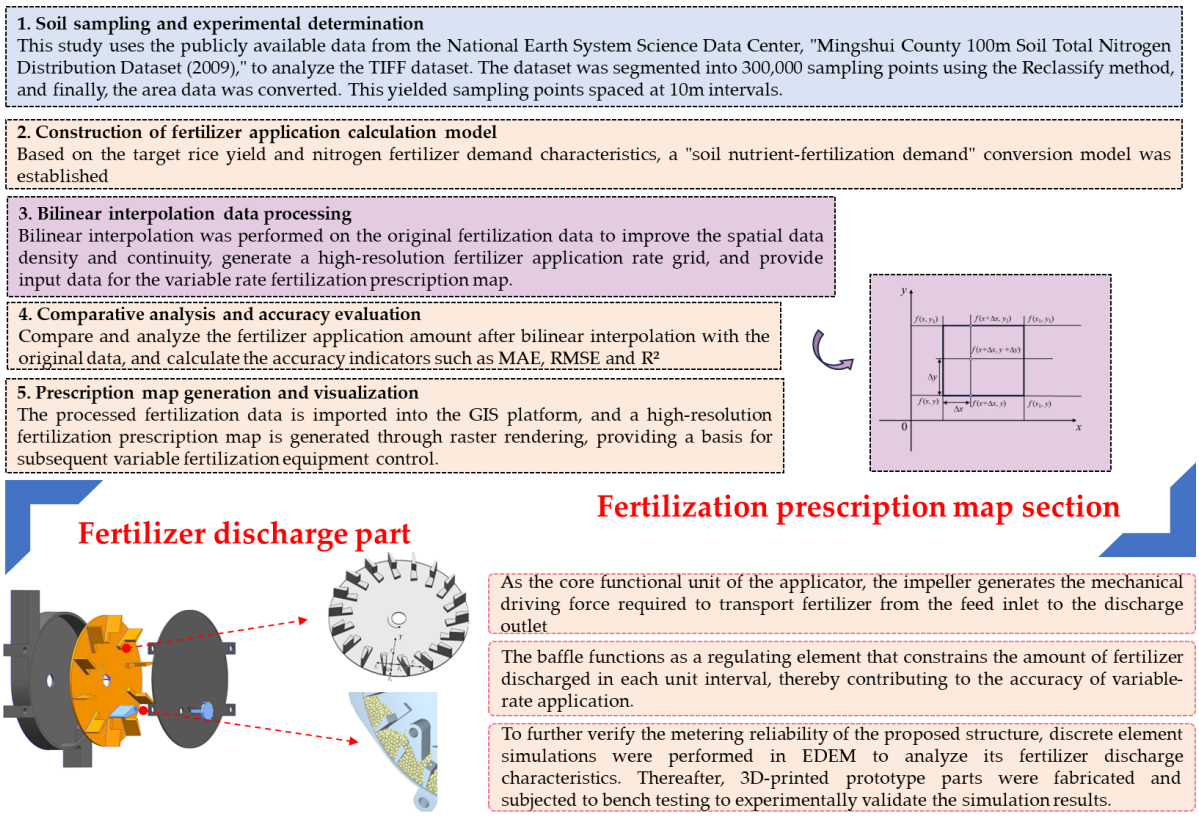

Fig. 1 - Flow chart

This algorithm supports presetting the target fertilization amount for each unit, thereby enabling fine management and control of fertilization operations. In summary, while different studies focus on various aspects such as sensor platforms, fertilization algorithms, and map generation methods, they all demonstrate that data-driven approaches are the core support for variable fertilization technology.

Fertilizer calculation

Since this study calculates soil fertilization rates using the widely adopted nutrient balance method, a grid size of 5 m × 5 m was selected to match both the soil sampling interval and the typical operating width of fertilization machinery in paddy fields. This grid resolution balances spatial accuracy and computational efficiency while meeting the practical requirements of variable-rate fertilization. To reduce field sampling workload, soil samples were collected using a 10 m × 10 m grid. However, directly assigning fertilization rates based on a single vertex value may lead to data discontinuity, which can adversely affect the smoothness of fertilization operations and the stability of the control system. To address this issue, bilinear interpolation was employed to calculate the fertilization rate at the grid center using the values of the four surrounding vertices, as shown in **Fig. 2**. By accounting for the relative position of the center point within the grid, this method provides a more accurate estimation of the central value, thereby improving the spatial continuity and operational feasibility of the prescription map.

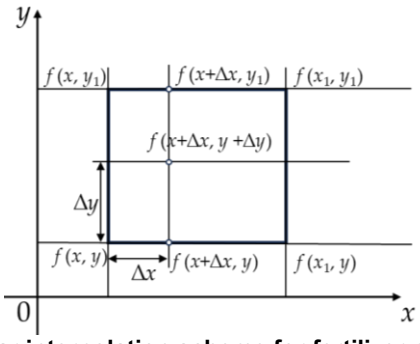

Fig. 2 - Bilinear interpolation scheme for fertilizer rate calculation

$$f(x+\Delta x, y) = \left(x_1 - x - \Delta x\right) f(x, y) + \Delta x f(x_1, y) \quad (1)$$

$$f(x+\Delta x, y_1) = \left(x_1 - x - \Delta x\right) f(x, y_1) + \Delta x f(x_1, y_1) \quad (2)$$

$$f(x+\Delta x, y+\Delta y) = \left(y_1 - y - \Delta y\right) f(x+\Delta x, y) + \Delta y f(x+\Delta x, y_1) \quad (3)$$

Since a 10 m grid spacing was used, the interpolation offsets Δx and Δy were both 5 m in the bilinear interpolation calculation.

$$f(x+5, y+5) = 5\left(y_1 - 5\right) f(x, y) + 5(y_1 - 5) f(x_1, y) + 25 f(x, y_1) + 25 f(x_1, y_1) \quad (4)$$

Subsequently, the sampled data and the results obtained from interpolation are analyzed to determine whether the interpolated results can be used as data for generating the prescription map.

Data analysis and prescription chart creation

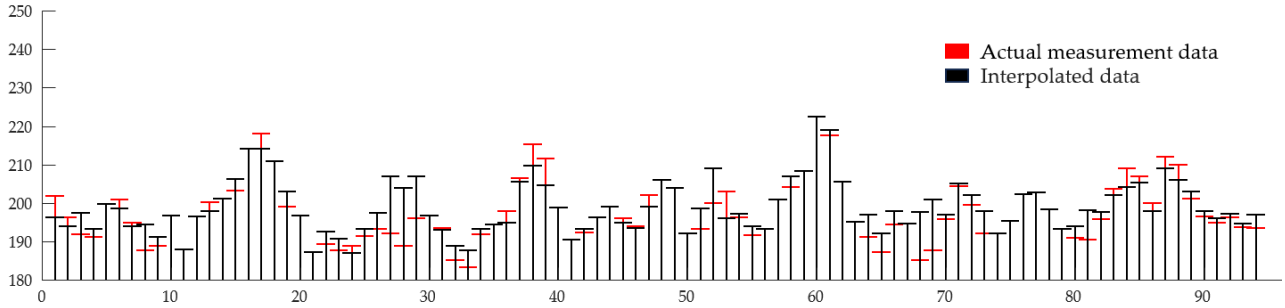

Fig. 3 - Comparison of bilinear interpolation and actual measured fertilizer amount

Fig. 3 shows the comparison between fertilization amounts from bilinear interpolation and the actual measured values. To evaluate the accuracy of bilinear interpolation and conventional Kriging in generating prescription maps, this study used MATLAB 2024a to calculate three metrics: *RMSE*, *MAE*, R^2 for both data sets. The results show that the prescription map generated by bilinear interpolation combined with Kriging has

good fitting accuracy, with an *MAE* of 2.61, an *RMSE* of 4.2, and an R^2 of 0.74. The low MAE and RMSE indicate small prediction errors, and the method can describe the spatial distribution of soil nutrients well, even with limited sampling points. This also shows that bilinear interpolation improves spatial continuity and supports variable fertilization. The RMSE still shows some deviation, meaning accuracy decreases in certain areas.

$$MAE = \frac{1}{n}\sum_{i=1}^{n}\left|y_c - y\right| \tag{5}$$

$$RSME = \sqrt{\frac{1}{n}\sum_{i=1}^{n}(y_c - y)^2} \tag{6}$$

$$R^2 = 1 - \frac{\sum_{i=1}^{n}(y_c - y)^2}{\sum_{i=1}^{n}(y - \bar{y})^2} \tag{7}$$

where: y_c is the interpolated value, y is the measured value, $\bar{y}$ is the mean of measured values, n is the number of samples.

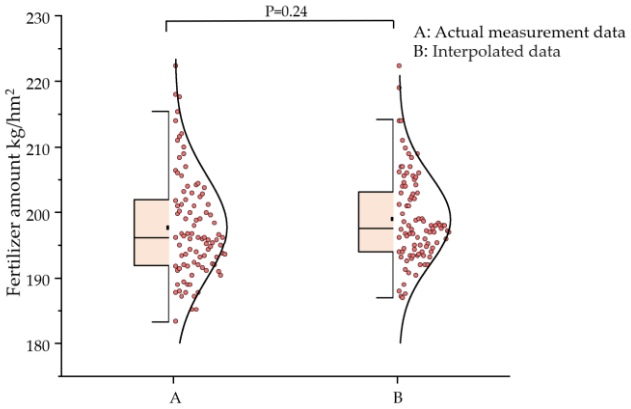

Fig. 4 - Test of mean difference of fertilizer application amount

To verify the differences in variance and mean between the two data sets, a T-test was conducted, and the results are shown in **Fig. 4.** The T-test yielded a p-value of 0.24, which is much greater than the critical value at the significance level ($p > 0.05$). This indicates that there is no significant difference in variance and mean between the two data sets, and the data overall exhibit good consistency and comparability. Therefore, it can be concluded that the two samples likely come from the same population or have similar distribution characteristics, and the subsequent analysis results are statistically valid.

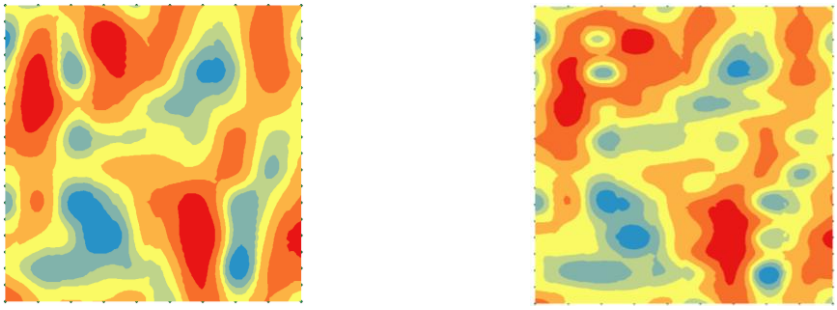

(a) (b)

Fig. 5 - Preparation of prescription map

(a) Interpolation result; (b) Actual result.

Bilinear interpolation has clear advantages in terms of prediction accuracy and spatial continuity. Without increasing the number of sampling points, it enhances data density, resulting in smoother boundaries and more gradual transitions in the prescription maps generated by Kriging. In addition, it allows a clearer representation of spatial variations in soil nutrients, providing a more reliable basis for precision fertilization decisions. However, this method also has certain limitations. Because it is based on a linear assumption, it may excessively smooth areas with rapid or abrupt changes in nutrient levels, thereby reducing the representation of actual spatial variability. Moreover, if the sampling points are unevenly distributed or the original data contain errors, these uncertainties may be amplified during the interpolation process, leading to

local prediction bias. The virtual points generated by interpolation may also affect the accuracy of semivariogram modeling.

The purpose of this subsection is to clarify the spatial distribution of soil nutrients and the corresponding fertilization range in the study area, providing a basis for subsequent fertilization device design. By comparing interpolated results with original sampling data, it is shown that bilinear interpolation produces more concentrated yet reasonable values, indicating practical applicability. Therefore, the Kriging fertilization prescription map with bilinear interpolation can serve as a reliable basis for variable fertilization decisions, supporting the feasibility of the device's control strategy and fertilization process.

STRUCTURE AND WORKING PRINCIPLE OF FERTILIZER APPLICATION DEVICE

The device consists primarily of components such as the housing (Outer shell, Cover plate), impeller, fertilizer adjustment baffle, and ratchet mechanism. Prior to operation, the device must be assembled, and the fertilizer inlet of the housing aligned with the discharge port of the fertilization machine's fertilizer tank. The housing is then securely fixed to the fertilization machine using bolts.

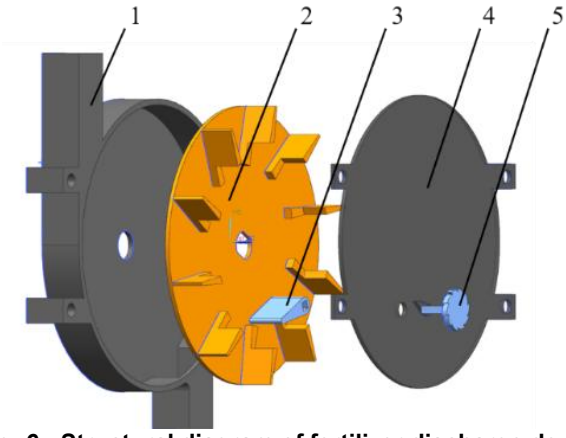

Fig. 6 - Structural diagram of fertilizer discharge device

1. Outer shell; 2. Impeller; 3. Fertilizer adjustment baffle; 4. Cover plate; 5. Ratchet.

During fertilization, fertilizer granules initially enter the device through the inlet and are subsequently conveyed to the impeller area. The impeller is driven by a transmission gear at the rear or by a bevel gear at the front. As the impeller rotates, its groove structure moves the fertilizer granules along a circular path. Upon reaching the fertilizer adjustment baffle, the baffle effectively blocked and regulate the flow of the fertilizer, enabling dynamic control of the fertilization rate. The baffle is connected to the housing via an axis and are integrated with the ratchet mechanism to limit movement to one direction, preventing vane failure due to reverse impacts or fertilizer accumulation. This feature enhances both the control precision and system stability. Finally, under the influence of gravity, the fertilizer naturally falls from the discharge port, completing the fertilization process.

Impeller design

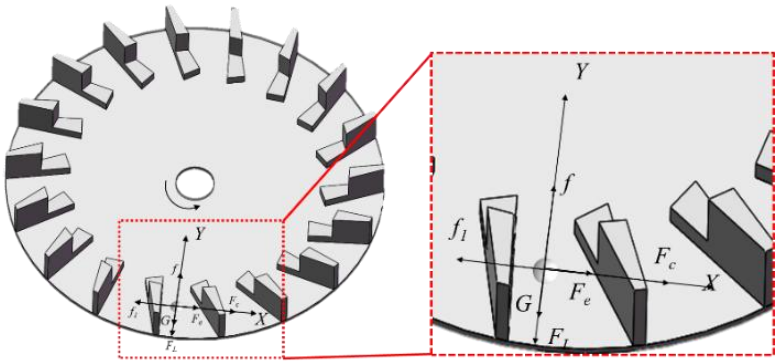

Fig. 7 - Mechanical analysis of fertilizer filling process

The impeller is the most critical component that enables the fertilizer dispenser to discharge fertilizer. The entire fertilization process relies on the rotation of the impeller to drive the discharge. Therefore, the diameter of the impeller, the height of the blades, and the number of blades all directly impact the discharge

performance of the device. To avoid difficulties in fertilizer discharge and poor uniformity caused by centrifugal force, rotational speed, and other factors, the structural parameters of the impeller are crucial, as they directly affect the force and movement of the fertilizer granules. Therefore, it is essential to establish a model of the impeller cross-section to analyze the forces acting on the fertilizer during its movement.

Fertilizer in the tank is concentrated at the upper inlet and falls into the fertilizer groove under its own weight. During the filling process, the relative velocity of the fertilizer granules is too high, causing the particles to flow towards one side of the groove, which negatively affects the filling process. Therefore, the factors influencing the relative velocity of the fertilizer were analyzed. A single fertilizer granule was then randomly selected for mechanical analysis, as shown in **Fig. 7.**

Based on the forces acting on the particles, a force balance equation is established, as follows:

$$\begin{cases} F = G + F_L + F_e + F_c + f_1 + f \\ F_c = 2m\omega v \\ F_L = m\omega_1 r^2 \end{cases} \quad (8)$$

where: F is the resultant force acting on the fertilizer granule, [N]; G is the gravitational force on the particle, [N]; F_L is the centrifugal force on particles, [N]; F_e is the inertial force, [N]; F_c is the Coriolis force, [N]; f_1 is the horizontal frictional force, [N]; f is the vertical frictional force, [N]; m is the mass of a single fertilizer granule, [kg]; ω is the angular velocity of the impeller, [rad/min]; v is the relative velocity between the fertilizer granule and the impeller, [m/s]; ω_1 is the relative angular velocity between the fertilizer granule and the impeller, [rad/min]; r is the radius from the fertilizer particle to the center of the impeller.

Based on the force analysis of the particles, the mechanical equilibrium equations in the vertical and horizontal directions are established. Further derivation leads to the calculation of the vertical acceleration an and horizontal acceleration am of the fertilizer granules, as follows:

$$\begin{cases} a_n = \dfrac{f_1 - 2m\omega v - m\omega_1^2 r}{m} \\ a_m = \dfrac{\varepsilon F_N}{m} \end{cases} \quad (9)$$

The result is obtained as follows:

$$v = e^{-2t\tau\omega}\left[\omega r + \frac{g(1-e^{2t\tau\omega})}{2\omega}\right] \quad (10)$$

where: τ is the friction coefficient between the granule and the impeller.

To ensure that the normal motion of the fertilizer granules remains unchanged, i.e., a_n=0, and given that the friction coefficient τ between the fertilizer granules and the device is 0.43, the range of impeller rotational speed ω can be determined based on the working forward speed v. The rotational speed ω is found to range from 60 to 120 rad/min. The filling performance of the device is related to the impeller angular velocity ω and the radius of the impeller's outer edge, which corresponds to the radius r of the fertilizer granules' center of mass. Here, r is taken to be 90 mm.

Design of fertilizer adjustment baffle

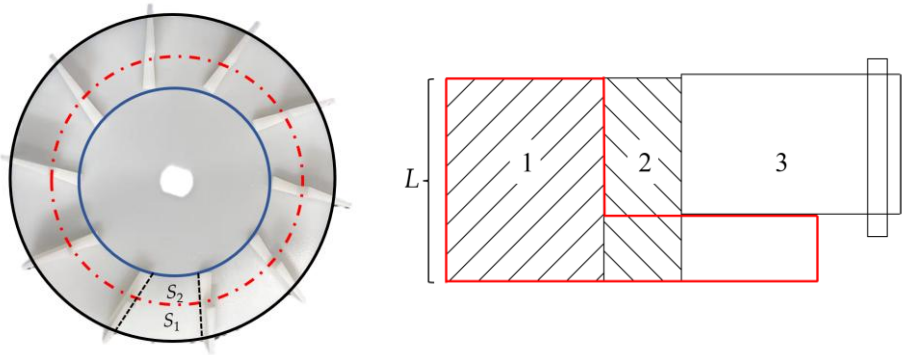

Fig. 8 - Diagram of the fertilizer adjustment and distribution plate operation

1. Active fertilization area (the red part); 2. Passive fertilization area; 3. Fertilizer adjustment paddle.

The fertilizer regulating baffle is one of the key components enabling the variable fertilization function of this device. It mainly consists of a baffle and a ratchet locking mechanism. The baffle adjusts the gap between itself and the impeller by rotating, thereby controlling the cross-sectional area through which the fertilizer flows. When the impeller rotates, it pushes fertilizer particles along the grooves towards the baffle area. Adjusting the gap allows for a certain degree of sorting and separation of the fertilizer, ensuring a more uniform distribution of fertilizer in each groove, thus achieving precise control.

The ratchet mechanism is designed to lock the position of the fertilizer adjustment baffle, ensuring that the baffle can only be adjusted in the preset direction. This prevents reverse movement of the baffle due to vibrations or fertilizer flow during fertilization, thereby maintaining stability. The size of the ratchet has a direct impact on the adjustment accuracy. In this study, an enlarged ratchet structure was modeled to more clearly illustrate the geometric features and working principle of the ratchet, though in practical assembly, it can be further miniaturized to match the overall system design.

The fertilizer in the impeller groove is divided into two parts based on the method of discharge. The portion of fertilizer pushed out by the fertilizing device is referred to as the active layer, while the fertilizer above the active layer, which is carried out due to friction, is referred to as the passive layer. The total fertilization amount P of the fertilizer dispenser is the sum of the active layer fertilization amount P_1 and the passive layer fertilization amount P_2, as shown in the following equation:

$$\begin{cases} P = P_1 + P_2 \\ P_1 = \dfrac{\sigma \rho z L S_1}{1000} \\ P_2 = \dfrac{\lambda \sigma \rho z L S_2}{1000} \end{cases} \quad (11)$$

where: σ is the fertilizer granule filling coefficient; ρ is the density of the fertilizer granules, [kg/m³]; z is the number of grooves; L_1 is the length of the highest impeller blade, [m]; S_1 is the cross-sectional area of the active fertilization zone, [m²]; λ is the characteristic coefficient of the passive layer of fertilizer granules; S_2 is the cross-sectional area of the passive fertilization zone, [m²].

EDEM simulation design and analysis

To study the performance impact of the fertilizer dispenser, simulation analysis is conducted using EDEM based on theoretical analysis.

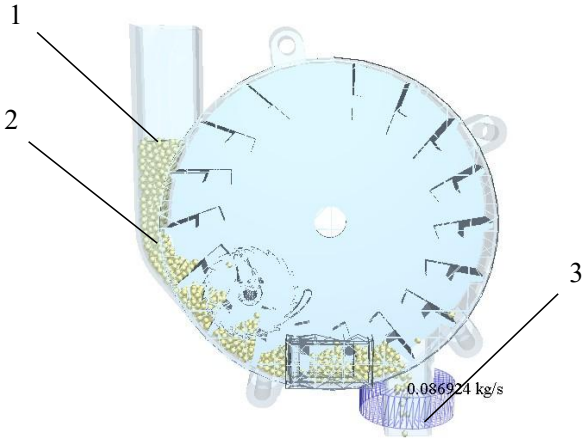

Fig. 9 - Simulation model

1. Pellet factory; 2. Pellets; 3. Flow monitoring area.

Since there is no adhesion between the fertilizer granules and the surface of the device, in order to reduce the number of particles generated and save simulation time, the particle generation rate is set to 3000 particles/s, with a total of 10,000 particles generated. The initial falling velocity of the particles is set to 2 m/s. The impeller rotational speeds are set to 40 r/min, 60 r/min, and 80 r/min, and the angle of the fertilizer adjustment baffle relative to the vertical direction is set to 35°.

During the simulation, a fixed time step of 2.1×10^{-6} s is set, which is 20% of the Rayleigh time step. The total simulation duration is 8 s, with simulation data saved every 0.01 s. The grid cell size is set to 6 times the average particle radius.

Table 1

Simulation parameter table

Item	Parameter	Value
Fertilizer	Density (kg/m^3)	1552
	Poisson's ratio	0.25
	Shear modulus (GPa)	0.096
Carbon steel	Density (kg/m^3)	7850
	Poisson's ratio	0.35
	Shear modulus (GPa)	210
Fertilizer- Fertilizer	Coefficient of restitution	0.075
	Static friction coefficient	0.372
	Kinetic friction coefficient	0.378
Carbon steel- Fertilizer	Coefficient of restitution	0.421
	Static friction coefficient	0.361
	Kinetic friction coefficient	0.382

To achieve more uniform fertilization, an analysis of the simulation process was conducted. It was found that a design issue in the fertilizer inlet pipe, which is too long and too narrow at the connection with the impeller, causes the fertilizer to enter the impeller at a speed higher than expected. This leads to fertilizer colliding with the blades, causing some of it to splash out, as shown in **Fig. 10**. Experimental observations show that the slower the impeller rotates, the more intense the splashing; the faster the impeller speed, the more stable the fertilization becomes.

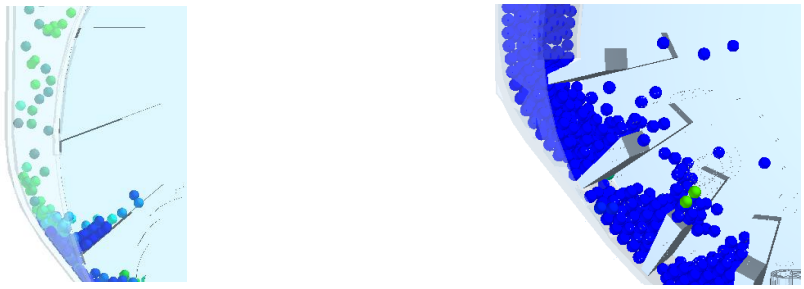

Fig. 10 - Simulation test results and analysis

BENCH TEST

The experiment was conducted in the High-Speed Rice Fertilization Performance Laboratory at Heilongjiang Bayi Agricultural University. The bench test setup is shown in the figure. The fertilizer used was compound fertilizer, with auxiliary tools such as an electronic scale and a measuring tape. During the test, the fertilization device was mounted on the test bench, and the conveyor belt speed was adjusted to simulate the forward movement of the implement. According to agronomic requirements, the conveyor belt speed was set within the range of 0.3~0.6 m/s.

Fig. 11 - Fertilization Rack Test Bench

The impeller rotational speed, machine forward velocity, and baffle opening angle were identified as key factors affecting fertilizer discharge. Impeller speed controls the discharge rate and distribution uniformity, influencing application consistency and response precision. Machine forward velocity must match the fertilizer feeding rate to maintain accurate application, as mismatches can cause over or under-fertilization and affect distribution stability.

The baffle opening angle governs the instantaneous mass flow through the discharge outlet, with adjustments made via a ratchet-based locking mechanism, where each tooth corresponds to a discrete angular change. Multiple levels of these factors were tested to evaluate their effects on fertilizer discharge and system performance. The primary objective of the experiment was to evaluate the fertilizer discharge coefficient of variation and the fertilizer omission rate of the designed device. Accordingly, three experimental factors were selected: impeller rotational speed (X_1), machine forward velocity (X_2), and baffle opening angle (X_3). The fertilizer discharge coefficient of variation (Y_1) and the fertilizer omission rate (Y_2) were designated as response indicators. The experiment aimed to investigate the individual and interactive effects of these factors on the response variables, thereby elucidating the influence mechanisms governing the stability and continuity of fertilizer application

$$x = \frac{\sum_{i=1}^{n} x_i}{n} \tag{12}$$

$$S = \sqrt{\frac{\sum_{i=1}^{n} (x_i - x)^2}{n-1}} \tag{13}$$

$$Y_1 = \frac{S}{x} \times 100\% \tag{14}$$

$$Y_2 = \frac{\sum_{i=1}^{k} L_i}{L} \times 100\% \tag{15}$$

where: x is the average total amount of fertilizer discharged, [g]; x_i is the amount of fertilizer discharged each time, [g]; S is the standard deviation of fertilizer discharge stability; Y_1 is the coefficient of variation of fertilizer discharge; Y_2 is the fertilizer breakage rate; L_i is the length of the i-th break (i=1, 2, 3...k), cm; L is the total length of fertilizer discharge, [mm].

Experimental Results

Data processing was performed using Design-Expert 13 software. A quadratic orthogonal design was established with impeller speed (X_1), implement forward speed (X_2), and baffle opening angle (X_3) as experimental factors, and fertilizer discharge coefficient of variation (Y_1) and fertilizer omission rate (Y_2) as response indicators. The factor coding table is shown in **Table 2**.

Table 2

Factor Level Coding Table

Coding	Impeller Rotational Speed (X_1)	Machine Forward Velocity (X_2)	Baffle opening angle (X_3)
-1.68	30	0.30	-72
-1	40	0.40	-36
0	50	0.50	0
1	60	0.60	36
1.68	70	0.70	72

The experimental design and results are shown in **Table 3.**

Table 3

Experimental Design and Results

NO.	Impeller Rotational Speed (X_1) / (rad/min)	Machine Forward Velocity (X_2) / (m/s)	Baffle opening angle (X_3) / (°)	Fertilizer discharge coefficient of variation Y_1 / (%)	Fertilizer omission rate Y_2 / (%)
1	-1	-1	-1	14.67	11.68
2	1	-1	-1	8.72	9.56
3	-1	1	-1	13.64	9.63
4	1	1	-1	12.89	8.84
5	-1	-1	1	13.92	10.42
6	1	-1	1	6.21	9.21
7	-1	1	1	12.93	10.42
8	1	1	1	13.64	8.46
9	-1.68	0	0	13.23	14.23

NO.	Impeller Rotational Speed (X_1) / (rad/min)	Machine Forward Velocity (X_2) / (m/s)	Baffle opening angle (X_3) / (°)	Fertilizer discharge coefficient of variation Y_1 / (%)	Fertilizer omission rate Y_2 / (%)
10	1.68	0	0	9.42	7.24
11	0	-1.68	0	10.26	15.64
12	0	1.68	0	12.87	8.68
13	0	0	-1.68	14.36	8.52
14	0	0	1.68	13.43	9.76
15	0	0	0	10.21	8.92
16	0	0	0	9.85	9.42
17	0	0	0	10.89	9.93
18	0	0	0	10.32	8.54
19	0	0	0	10.64	9.13
20	0	0	0	9.63	9.26
21	0	0	0	11.93	9.76
22	0	0	0	9.97	9.61
23	0	0	0	10.58	9.36
24	0	0	0	10.62	10.23
25	0	0	0	10.65	10.76

Analysis of variance was performed on the fertilizer discharge coefficient of variation and the fertilizer omission rate of the fertilization device. The results are presented in **Table 4.**

Table 4

Analysis of the coefficient of variation of fertilizer excretion

Source	Y_1: Coefficient of variation (%)				Y_2: Fertilizer omission rate (%)			
	Sum of squares	df	*F*	*P*	Sum of squares	df	*F*	*P*
Model	95.33	9	22.20	<0.0001**	52.20	9	3.81	0.0110*
X_1	29.61	1	62.05	<0.0001**	23.29	1	15.30	0.0014*
X_2	14.29	1	29.95	<0.0001**	16.97	1	11.15	0.0045*
X_3	1.68	1	3.51	0.0805	0.057	1	0.04	0.8487
X_1X_2	23.19	1	48.60	<0.0001**	0.042	1	0.03	0.8702
X_1X_3	0.011	1	0.02	0.88	0.01	1	0.01	0.9416
X_2X_3	1.36	1	2.85	0.11	0.51	1	0.34	0.5713
X_1^2	0.94	1	1.96	0.18	0.82	1	0.54	0.4736
X_2^2	1.72	1	3.61	0.0768	8.73	1	5.73	0.0302*
X_3^2	21.71	1	45.50	<0.001**	1.91	1	1.26	0.2797
Residuals	7.16	15			22.84	15		
Lack of fit	3.32	5	1.73		18.99	5	9.87	0.0013
Error	3.83	10			3.85	10		
Total	102.49	24			75.04	24		

Based on the bench test data, regression models were established with the fertilizer discharge coefficient of variation (Y_1) and the fertilizer omission rate (Y_2) as response variables.

As shown in **Table 4,** both models passed the overall significance test ($p < 0.05$). In terms of single-factor significance, for Y_1, the factors X_1, X_2, X_1X_2, and X_3^2 were highly significant; for Y_2, the factors X_1, X_2, and X_2^2 were significant. After removing the nonsignificant terms, the final response regression equations were obtained as follows.

$$\begin{cases} Y_1 = 10.49 - 1.47X_1 + 1.02X_2 + 1.70X_1X_2 + 1.15X_3^2 \\ Y_2 = 9.56 - 1.31X_1 - 1.11X_2 + 0.73X_2^2 \end{cases} \quad (16)$$

To visually analyze the interaction effects of impeller rotational speed (X_1), machine forward velocity (X_2), and baffle opening angle (X_3) on the fertilizer discharge coefficient of variation (Y_1) and the fertilizer omission rate (Y_2), response surface plots were generated using Design-Expert software, illustrating how these factors and their interactions influence Y_1 and Y_2, as shown in the figure.

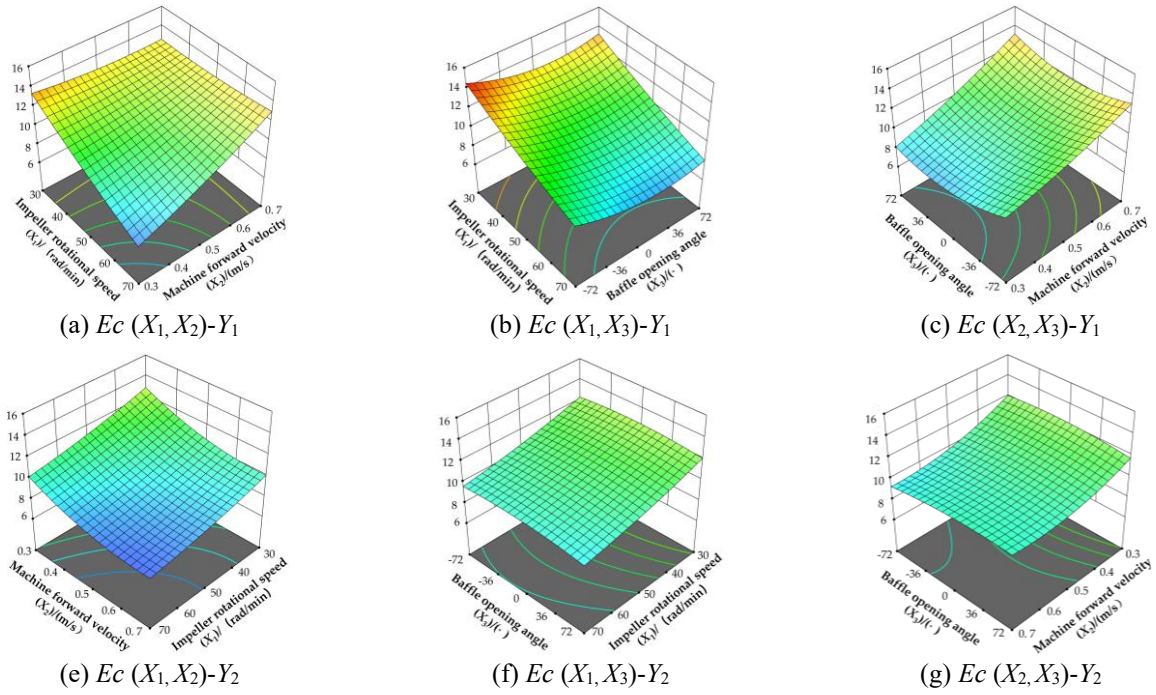

(a) Ec (X_1, X_2)-Y_1 (b) Ec (X_1, X_3)-Y_1 (c) Ec (X_2, X_3)-Y_1

(e) Ec (X_1, X_2)-Y_2 (f) Ec (X_1, X_3)-Y_2 (g) Ec (X_2, X_3)-Y_2

Fig. 12 - factors affecting the fertilizer discharge coefficient of variation and the Fertilizer Omission Rate

Fig. 12 illustrates the effects of different combinations of impeller rotational speed, machine forward velocity, and baffle opening angle on the fertilizer discharge coefficient of variation and the fertilizer omission rate. For the coefficient of variation, when the baffle angle is fixed at the 0 level -72° and impeller speed is constant, increasing forward velocity leads to a progressive rise in variation. Conversely, at fixed forward velocity, increasing impeller speed reduces variation, while varying the baffle angle at constant impeller speed results in a rise-then-fall trend. For the omission rate, with the baffle angle at 0 and impeller speed fixed, increasing forward velocity gradually decreases omission, and increasing impeller speed at fixed forward velocity also lowers omission. When the baffle angle varies at constant impeller speed, the omission rate remains generally stable, showing minimal fluctuation. Overall, forward velocity and baffle angle interactions strongly affect discharge variation, while higher impeller speeds improve uniformity and reduce omission.

To achieve stable fertilization performance, a multi-objective optimization was conducted using Design-Expert software, with the minimization of the fertilizer discharge coefficient of variation as the primary objective. The optimization targets and conditions were set as follows:

$$\begin{cases} \max Y_1(X_1, X_2, X_3) \\ \min Y_2(X_1, X_2, X_3) \\ s.t. \begin{cases} 30 < X_1 < 70 \\ 0.3 < X_2 < 0.7 \\ -72 < X_3 < 72 \end{cases} \end{cases} \quad (17)$$

Analysis of the optimized operational performance of the fertilization device determined the optimal combination of operational and structural parameters as follows: impeller rotational speed of 65.6 rad/min, implement forward speed of 0.39 m/s, and baffle opening angle of 54°. Under this configuration, performance tests showed a fertilizer discharge coefficient of variation of 8.54% and a fertilizer strip rate of 9.16%, meeting the agronomic requirements for intermittent deep-side fertilization specified in NY/T1003-2006.

CONCLUSIONS

(1) In this study, bilinear interpolation was applied to smooth abrupt changes in nutrient data in order to enhance spatial continuity, and the rationality of the interpolation was verified through data analysis.

(2) Based on the calculated fertilizer application rates, a variable impeller fertilization device was developed. A regression model relating the coefficient of variation of fertilizer application and the omission rate was established using the response surface methodology.

(3) Analysis of variance showed that all factors and their interactions had significant effects on both indicators, and the models showed good fit, so they could be used to predict and optimize fertilization performance. Multi-objective optimization then gave the best operating parameters: an impeller speed of 65.6 rad/min, a forward speed of 0.39 m/s, and a baffle opening of 54°. Under these settings, bench tests showed a fertilizer variation of 8.54% and an omission rate of 9.16%. These results show that the device works well and is stable for precision fertilization.

ACKNOWLEDGEMENT

This research was supported by the National Key R&D Program of China (2024YFD2300104); the Heilongjiang Province Postdoctoral Research Funding Project (LBH-Z20203); and the Key Laboratory of Resource Recycling Technology and Model, Ministry of Agriculture and Rural Affairs- “Cow Manure-Based Matrix Rice Nutrient Seedling Tray Forming Technology” (KLTMCUAR2024-01).

REFERENCES

[1] Bin Rahman., Zhang J. (2023). Trends in rice research: 2030 and beyond. *Food and Energy Security*, *12*(2), e390.

[2] Li L., Tian H., Zhang M.H., Fan P.S., Liu H.D., Chen X.F., Duan M.Y., Tang X.R., Wang Z.M. (2021). Deep placement of nitrogen fertilizer increases rice yield and nitrogen use efficiency with fewer greenhouse gas emissions in a mechanical direct-seeded cropping system. *The Crop Journal*, *9*(6), 1386–1396.

[3] Muthayya S., Sugimoto J.D., Montgomery S., Maberly G. (2014). An overview of global rice production, supply, trade, and consumption. *Annals of the New York Academy of Sciences*, *1324*(1), 7–14.

[4] Xu X., Xie J., Hou Y., He P., Mirasol F., Zhao S.C., Qiu S.J., Adrian M., Zhou W. (2015). Estimating nutrient uptake requirements for rice in China. *Field Crops Research*, *180*, 37–45.

[5] Liang Y., Bing S. (2016). Nutrient uptake requirements with increasing grain yield for rice in China. *Journal of Integrative Agriculture*, *15*(4), 907–917.

[6] Sohail D. (2024). Advancements in precision fertilization technologies and controlled-dispersion fertilizers for sustainable rice cultivation. *International Journal of Agriculture and Sustainable Development*, *6*(1), 29-42.

[7] Brambilla M., Elio R., Pietro T., Maurizio C., Marcello B., Carlo B. (2021). From conventional to precision fertilization: A case study on the transition for a small-medium farm. *Agri Engineering*, *3*(2), 438-446.

[8] Niu K., Bai S., Zhou L., Zhao B., Liu L.J., Yuan Y.W., Yuan D.Q., Xiong S., Zhang W.P. (2021). Design and experimental research of variable formula fertilization control system based on prescription diagram. *Applied Sciences*, *12*(1), 325.

[9] Zhou W., An T., Wang J., Fu Q., Wen N., Sun X.B., Wang Q., Liu Z. (2023). Design and experiment of a targeted variable fertilization control system for deep application of liquid fertilizer. *Agronomy*, *13*(7), 1687.

[10] Martí J.K., Català F.M., Tomàs N., Marta S.L. (2025). Mid-season variable-rate algorithm for organic and mineral rice fertilization. *Agronomy for Sustainable Development*, *45*(2), 13.

[11] Yu F., Bai J., Jin Z., Zhang H.G., Guo Z.G., Chen C.L. (2022). Research on precise fertilization method of rice tillering stage based on UAV hyperspectral remote sensing prescription map. *Agronomy*, *12*(11), 2893.

[12] Shin J., Won J., Kim S.M., Kim D.C., Cho Y.J. (2023). Fertilization mapping based on the soil properties of paddy fields in Korea. *Agriculture*, *13*(11), 2049.

[13] Yu F.H., Cao Y.L., Xu T.Y., Guo Z.H., Wang D.K. (2020). Precision fertilization by UAV for rice at tillering stage in cold regions based on hyperspectral remote sensing prescription maps. *Transactions of the Chinese Society of Agricultural Engineering*, *36*, 103–110.

[14] Lösch M., Schmidhalter U. (2023). Improving the congruency of satellite-based fertilizer maps with field-operable units using pneumatic spreaders. *Precision Agriculture*, *24*(4), 1312–1332.

[15] Qi X.., Zhou Z.., Yang C., Luo X.., Gu X.., Zhang Y., Liu W. (2016). Design and experiment of key parts of pneumatic variable-rate fertilizer applicator for rice production. *Transactions of the Chinese Society of Agricultural Engineering*, *32*(6), 20–26.

[16] Su N., Xu T., Sun L., Wang R., Wei Y. (2015). Variable-rate fertilization system with adjustable active feed-roll length. *International Journal of Agricultural and Biological Engineering*, *8*(4), 19–26.

[17] Da Silva M.J., Magalhães P.S.G. (2019). Modeling and design of an injection dosing system for site-specific management using liquid fertilizer. *Precision Agriculture*, *20*(4), 649–662.
[18] Lin Y., Sun L., Chen D., Zhu G., Kong Z., Yu G. (2025). Design and optimization of a terminal shunting acceleration device for rice side deep fertilization. *Chinese Journal of Rice Science*, *39*(4), 451.
[19] Radočaj D., Jurišić M., & Gašparović M. (2022). The role of remote sensing data and methods in a modern approach to fertilization in precision agriculture. *Remote Sensing*, *14*(3), 778.
[20] Miao C., Wang Y. (2024). Interpolation of non-stationary geo-data using Kriging with sparse representation of covariance function. *Computers and Geotechnics*, *169*, 106183.